Optimal timing of tau pathology imaging and automatic extraction of a reference region using dynamic [18F]THK5317 PET

My Jonasson[a,b,*], Anders Wall[a,c], Konstantinos Chiotis[e], Antoine Leuzy[e], Jonas Eriksson[c,d], Gunnar Antoni[c,d], Agneta Nordberg[e,f], Mark Lubberink[a,b]

[a] Department of Surgical Sciences, Uppsala University, Uppsala, Sweden
[b] Medical Physics, Uppsala University Hospital, Uppsala, Sweden
[c] Department of Medicinal Chemistry, Uppsala University, Uppsala, Sweden
[d] PET Centre, Uppsala University Hospital, Uppsala, Sweden
[e] Division of Clinical Geriatrics, Center for Alzheimer Research, Department of Neurobiology, Care Sciences and Society, Karolinska Institutet, Huddinge, Sweden
[f] Theme Aging, Karolinska University Hospital, Huddinge, Sweden

ARTICLE INFO

ABSTRACT

[18F]THK5317 is a PET tracer for *in-vivo* imaging of tau associated with Alzheimer's disease (AD). This work aimed to evaluate optimal timing for standardized uptake value ratio (SUVR) measures with [18F]THK5317 and automated generation of SUVR-1 and relative cerebral blood flow (R_1) parametric images. Nine AD patients and nine controls underwent 90 min [18F]THK5317 scans. SUVR-1 was calculated at transient equilibrium (TE) and for seven different 20 min intervals and compared with distribution volume ratio (DVR; reference Logan). Cerebellar grey matter (MRI) was used as reference region. A supervised cluster analysis (SVCA) method was implemented to automatically generate a reference region, directly from the dynamic PET volume without the need of a structural MRI scan, for computation of SUVR-1 and R_1 images for a scan duration matching the optimal timing. TE was reached first in putamen, frontal- and parietal cortex at 22 ± 4 min for AD patients and in putamen at 20 ± 0 min in controls. Over all regions and subjects, $SUVR_{20-40}$-1 correlated best with DVR-1, $R^2 = 0.97$. High correlation was found between values generated using MRI- and SVCA-based reference ($R^2 = 0.93$ for $SUVR_{20-40}$-1; $R^2 = 0.94$ for R_1). $SUVR_{20-40}$ allows for accurate semi-quantitative assessment of tau pathology and SVCA may be used to obtain a reference region for calculation of both SUVR-1 and R_1 with 40 min scan duration.

1. Introduction

Alzheimer's disease (AD) is characterized by a cascade of complex pathophysiologic processes including deposition of amyloid-beta plaques, accumulation of tau in the form of neurofibrillary tangles, and neurodegeneration. Because of the close association between tau pathology, neurodegeneration and cognitive impairment (Okamura et al., 2014), there is increasing interest in the development of positron emission tomography (PET) tracers that bind specifically to tau (Villemagne et al., 2015). [18F]THK5317 is a well-characterized tau-specific tracer (Jonasson et al., 2016; Okamura et al., 2013; Lemoine et al., 2015; Chiotis et al., 2018), showing high retention in patients with AD with a regional uptake pattern matching that of the distribution of tau pathology described by post-mortem studies (Chiotis et al., 2016). There has been some concern about binding of tau tracers such

as the structurally related tracer [18F]THK5351 to monoamine oxidase-B (MAO-B) present in astrocytes (Ng et al., 2017). A recent *in vitro* study of the racemic compound [3H]THK5117 showed relatively low affinity to monoamine oxidase-B indicating that competitive binding of the corresponding (*S*)-enantiomer [18F]THK5317 would not present a problem at the concentrations encountered during clinical PET studies (Lemoine et al., 2017), although *in vivo,* an off target binding is evident in the basal ganglia (Chiotis et al., 2016).

Use of tau imaging in clinical practice for diagnostic purposes, study of disease progression and evaluation of drug treatment effects, as well as in research investigations with PET, is facilitated by short scans and simplified analysis methods. Previous studies, however, have shown a poor correlation between static standardized uptake value ratio (SUVR) at various late time intervals and binding potential BP_{ND} based on dynamic scans with [18F]THK5317 in AD patients (Jonasson et al., 2016).

* Corresponding author at: Medical Physics, Uppsala University Hospital, 751 85 Uppsala, Sweden.
  E-mail address: my.jonasson@radiol.uu.se (M. Jonasson).

The optimal time for assessment of SUVR, in terms of its agreement with the non-displaceable binding potential (BP_{ND}), is at peak specific binding, or transient equilibrium (TE), when theoretically SUVR-1 equals BP_{ND} (Ito et al., 1998). However, for all tau tracers of which, to our knowledge, tracer kinetic studies in humans have been described ([18F]THK5317 (Jonasson et al., 2016), [18F]THK5351 (Lockhart et al., 2016), [18F]AV-1451 (Golla et al., 2017; Hahn et al., 2017), [18F]MK6240 (Lohith et al., 2017)) TE is reached at different time points throughout the brain, resulting in a spatially varying bias in SUVR values compared to BP_{ND} values. In addition to being spatially varying, binding characteristics in regions with tau accumulation will change over time This may result in a disease progression-dependent bias in SUVR, complicating between group comparison of SUVR values in both cross-sectional and longitudinal studies.

In addition to measures of tau accumulation, dynamic [18F]THK5317 can also provide estimates of the relative tracer delivery (R_1), the ratio between K_1 in the target and reference region, reflecting relative regional cerebral blood flow if extraction in both region is similar. A recent study has shown that [18F]THK5317 R_1 values demonstrate a high correlation to [18F]FDG cerebral glucose metabolism (Rodriguez-Vieitez et al., 2017). However, in that study, the R_1 values were only validated using a scan length of 60 min and use of R_1 possibly based on shorter scan durations, matching the optimal timing for SUVR measurements, needs to be validated.

A step to further simplify the analysis method is the availability of an automatic way to define the reference region volume of interest (VOI) directly from the dynamic PET data, without the need of a structural MRI or the use of manual VOI delineation. One approach for this is the supervised cluster analysis (SVCA) method. The SVCA algorithm segments voxels in the dynamic PET volume based on their time activity curves (TACs) with no spatial constraint, i.e. the whole brain is considered. Voxels with kinetic behaviour most resembling the TACs of the proposed reference region are included in the reference VOI. The SVCA method has been suggested as an automatic way of extracting a reference region in previous studies for (R)-[11C]PK11195 (Turkheimer et al., 2007; Yaqub et al., 2012), [11C]PIB (Ikoma et al., 2013), (R)-[11C]rolipram (Lyoo et al., 2014), [11C]TMSX (Rissanen et al., 2015) and [11C]PE2I (Jonasson et al., 2017). Although the principles of an implementation of the SVCA algorithm are similar for each tracer, this method needs to be validated for [18F]THK5317.

The purpose of the present work was to determine time to TE for various brain regions, to quantify the time-depending biases in different tissues for healthy controls (HC) and AD patients, and to establish the optimal time window for measurement of SUVR and R_1 of [18F]THK5317. In addition, the present work aimed to validate a SVCA method for automatic extraction of a reference TAC directly from the dynamic [18F]THK5317 data.

2. Methods

2.1. Subjects

Data from 18 subjects, including nine AD patients and nine HCs included in a previously published study (Jonasson et al., 2016; Chiotis et al., 2016) was used in the present work. Eight of the subjects (4 AD and 4 HC) were included to serve as a separate set of data for the definition of kinetic classes in the SVCA algorithm. Patient characteristics were previously described in detail (Chiotis et al., 2016). All subjects signed an informed consent before inclusion and the Regional Board of Medical Ethics in Stockholm and the Medical Radiation Ethics Committee at Uppsala University Hospital approved the study.

2.2. Data acquisition

The radiosynthesis of [18F]THK5317, the (S)-enantiomeric form of [18F]THK5117, has been described previously (Jonasson et al., 2016).

All subject underwent a [18F]THK5317 PET scan on an ECAT Exact HR + scanner (Siemens, Knoxville) (Brix et al., 1997). After a 10 min transmission scan with rotating ^{68}Ge rod sources, the scan was started simultaneously with the injection of 3 MBq/kg [18F]THK5317. Ten of the subjects (five AD and five HC) underwent a 90 min dynamic PET scan (25 frames; 6×10, 3×20, 2×30, 2×60, 2×150, 4×300, and 6×600 s), while the remaining subjects underwent a 60 min dynamic scan (22 frames; 6×10, 3×20, 2×30, 2×60, 2×150, 4×300, and 3×600 s). These last 8 subjects were only used for definition of the kinetic classes applied in SVCA. Images were reconstructed using normalisation- and attenuation-weighted ordered subsets expectation maximisation (6 iterations, 8 subsets) with a 4 mm Hanning post-filter, applying all appropriate corrections for attenuation, scatter, randoms, etc., as included in the scanner software. In addition, all subjects underwent a T1-weighted structural MRI scan.

2.3. Volumes of interest

Dynamic PET images were corrected for motion using frame-by-frame realignment in Voiager software (GE Healthcare, Uppsala, Sweden). The T1-weighted MRI scans were co-registered to a summation image (0–5 min) of their corresponding PET volume and segmented into grey matter, white matter and CSF using SPM8 (Wellcome Trust Center for Neuroimaging, University College London, UK). VOIs were defined on the MRI images using a probabilistic atlas (PVElab)(Svarer et al., 2005) and projected onto the dynamic PET images to extract regional TACs. VOIs included in the analysis were: midbrain, hippocampus, amygdala, thalamus, putamen, sensory motor, occipital, entorhinal, frontal, temporal and parietal cortex Left and right side VOIs were averaged. In addition, a white matter VOI and a whole brain grey matter VOI were included, and a grey matter cerebellar VOI as reference region.

2.4. Optimal timing

DVR-1 values were calculated on a VOI-basis, using the reference Logan method (30–90 min) (Logan et al., 1996) with cerebellar grey matter as reference tissue, which was previously shown to agree well with plasma input-based analysis (Jonasson et al., 2016). For each VOI, the time at which TE occurred was determined as the peak of the specific binding curve, calculated by subtraction of the grey matter cerebellum TAC from the VOI TAC. To account for differences in the delivery between target regions and cerebellum, the target TAC was scaled by the ratio of the radioactivity concentrations in cerebellum and target between 1 and 2 min post-injection (p.i). Noise-induced peaks in specific binding at early time points (< 15 min) were avoided by only allowing TE values larger than 15 min. SUVR-1 was calculated for all VOIs for seven consecutive fixed 20 min intervals between 10 and 90 min p.i., in steps of 10 min, as well as for a 20 min interval centred around TE. Correlation and bias between SUVR-1 values for the various time intervals and DVR-1 were calculated using linear regression. Cohen's d was calculated as the difference between the means of both groups (AD patients and HCs) divided by the pooled standard deviation. This was calculated for both SUVR-1 values at TE and different time intervals, as well as DVR-1, in amygdala, parietal-, temporal- and entorhinal cortex. This gives the effect size expressed in number of pooled standard deviations and gives a further indication of the ability to discriminate between the two groups for different time intervals of the calculations.

Parametric SUVR-1 images for the fixed time intervals were generated, and DVR-1 images were constructed using the reference Logan method (30–90 min). In addition, time to TE images were computed based on specific binding curves estimated using receptor parametric mapping (RPM) (Gunn et al., 1997), which is a basis function implementation of the simplified reference tissue model (SRTM) (Lammertsma & Hume, 1996).

2.5. Supervised cluster analysis

A set of four kinetic classes were predefined on dynamic [^{18}F]THK5317 data from eight subjects (4 AD and 4 HC) that were specifically included for this purpose only: cerebellar grey matter, grey matter, white matter and a blood pool class. The cerebellum class was defined on the HC subjects, to ensure that only healthy tissue was included, using the VOIs generated with PVElab for each subject. The grey matter, white matter and blood pool classes were defined on the AD patients; grey matter and white matter were defined using the PVElab VOIs and the blood pool class was defined as voxels with a value higher than 20% of the maximum voxel value during the initial 60 s (frame 1–6) on the 10 most caudal slices. The definition of the classes other than cerebellum was aimed at avoiding inclusion of their associated voxels in the cerebellum class. The TACs from each class were normalized to their respective area under the curve. The SVCA algorithm, specific for [^{18}F]THK5317, was implemented in Matlab (Mathworks, Natick MA).

To generate reference time-activity curves for the 5 AD patients and the 5 HC subjects included in the validation of the method, TACs of each voxel in the dynamic data sets were normalized to their area under the curve. A non-negative least-squares algorithm was used to find a linear combination of the probability for each voxel to correspond to each kinetic class. Four different thresholds, as a limit of the probability of the voxels to belong to a class, were investigated: 0.3, 0.4, 0.5 and 0.6. Voxels with a probability higher than the threshold were assigned to that specific class. The voxels selected for the cerebellum class were regarded as reference region and a mean of the TACs of the selected voxels was calculated to extract a reference TAC. The SVCA-extracted reference TAC was then used as input function to generate new parametric SUVR-1 images for the optimal time window as well as R_1 images using RPM. RPM was implemented with 100 basis functions predefined for each scan, with discrete values for the exponential variable ranging from 0.005 to 0.5 min^{-1}, and R_1 was calculated using data ranging from the start of the scan to the end of the optimal time window for SUVR measures. Regionally averaged voxel values of the 11 VOIs were extracted from the SUVR-1 images and compared with the SUVR-1 values calculated using an MRI-based cerebellum reference for the optimal timing. Similarly, values extracted from RPM R_1 parametric images were compared with regional SRTM R_1 generated for the full 90 min scan duration with an MRI-based reference. Values were compared using linear regression and the square of the correlation coefficient (R^2). In addition, Cohen's d was calculated between the AD and HC groups for the SUVR-1 values of the optimal time window in amygdala, parietal-, temporal- and entorhinal cortex.

3. Results

3.1. Optimal timing

Mean parametric images of reference Logan DVR-1 and SUVR-1 for time intervals of 20–40 and 70–90 min, are given in Fig. 1 for the AD and HC groups. There is an obvious overestimation of SUVR-1 values compared to DVR-1, and an increase of SUVR-1 with increasing time.

Fig. 2(a) shows parametric maps of the mean time to TE in AD and HC subjects, as well as the difference between the two groups. The parametric maps clearly show the decreased time to TE in AD patients in occipital, parietal and sensory motor cortices. Fig. 2(b) shows mean time to TE for all investigated VOIs. For AD patients, TE was reached first in the putamen, frontal- and parietal cortex at 22 ± 4 min (mean ± SD), whereas in HCs, TE was reached first in putamen at 20 ± 0 min. In AD, TE in temporal cortex was reached at 24 ± 5 min. TE was reached last in occipital cortex for both AD patients and HCs at 52 ± 23 and 80 ± 0 min respectively. Mean time to TE across the whole brain was 30 ± 0 min in AD and 42 ± 4 min in HC (p < .05). Fig. 3 shows correlation (a-b) and bias (c-d) between SUVR-1 and
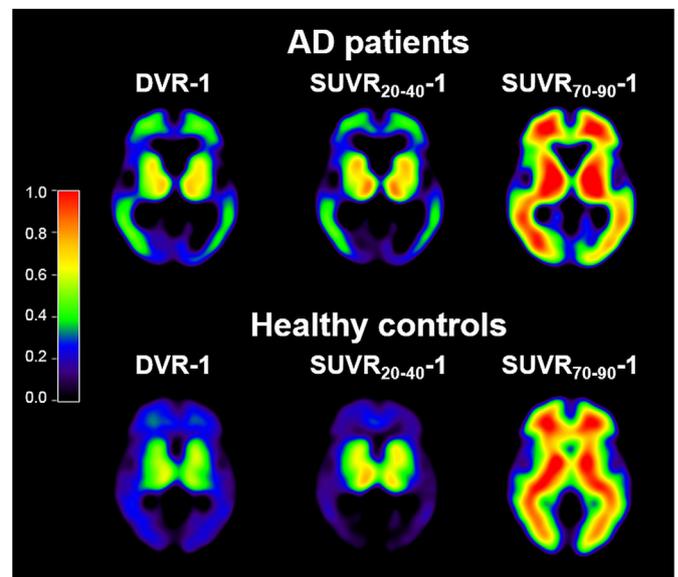

Fig. 1. Mean [^{18}F]THK5317 reference Logan DVR-1 and SUVR-1 images for the 20–40 and 70–90 min intervals for the AD patients and the HCs.

DVR-1 for AD and HC subjects, as well as the difference in bias between AD and HC (d), for all investigated regions. Over all regions and subjects, SUVR-1 on a time interval centred around 30 or 40 min showed a high correlation with DVR-1 (R^2 = 0.97 and 0.95 respectively for both AD patients and for HC). The lowest mean bias for the fixed intervals was found for the 20–40 min time interval (2% for both AD and HC). This suggests an overall preference for an SUVR time window centred around 30 min, both in terms of correlation and bias relative to DVR-1. In HCs, there is a clear grouping in bias in two groups of regions, with cortical regions showing less bias and less time dependence of bias than limbic regions and putamen. This difference is less obvious in the AD group. Use of SUVR$_{TE}$-1 resulted in somewhat lower correlations with DVR-1 (R^2 = 0.87 and 0.86 in AD and HC, respectively), but a bias equal to the 20–40 min time interval (2%) in AD patients. The bias in SUVR is higher in AD patients than in HC and difference in bias between the groups is generally smallest for a window centred around 30 min p.i.

Cohen's d of DVR-1 and SUVR-1 at TE and different time intervals, for amygdala, parietal-, temporal- and entorhinal cortex, between AD patients and HCs are shown in Fig. 4. For time windows centring at 30 min and higher, Cohen's d was close to constant in parietal-, temporal- and entorhinal cortices, with the highest values, around 5, for parietal cortex. In the amygdala, Cohen's d showed a continuing increase for increasing time after injection even at 80 min p.i.

3.2. Supervised cluster analysis

Since an overall preference for SUVR calculation was found for a time window centred around 30 min, *i.e.* 20–40 min, only this interval was used when investigating the SVCA for SUVR and a total scan duration of 0–40 min for R_1 measures.

Mean residual sum of squares (RSS) for all subjects was lowest for a threshold of 0.3 and increased with increasing thresholds. The correlation between SUVR-1 with MRI and SVCA-based reference regions were highest for thresholds of 0.4 and 0.5 (R^2 = 0.93 and 0.94, respectively). Given that the lowest bias was seen using the 0.5 threshold (0.01) this threshold was chosen for further evaluation.

The normalized TACs of the predefined classes used in the SVCA algorithm are given in Fig. 5(a). Fig. 5(b) shows the MRI-based cerebellum reference region obtained using PVElab. Fig. 5(c) shows the reference region extracted using SVCA and VOIs of the remaining SVCA
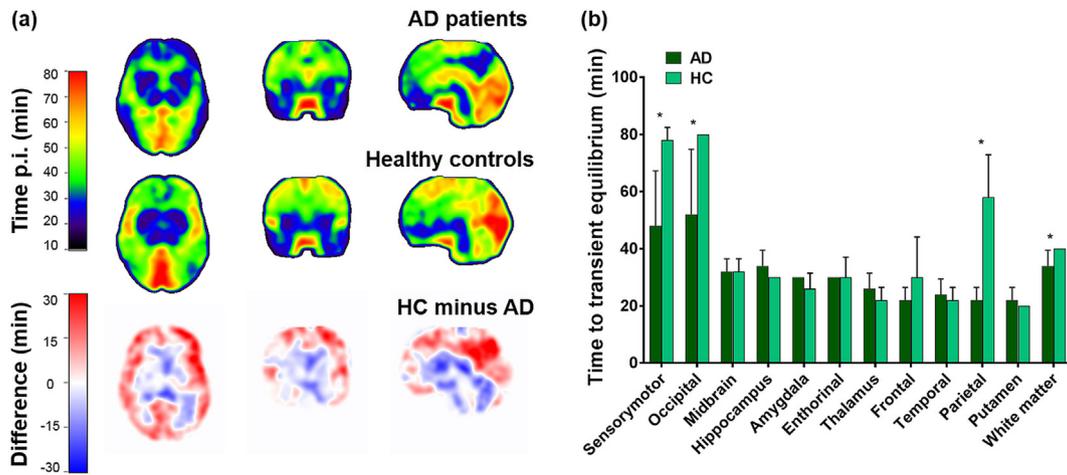
Fig. 2. (a) Mean time to transient equilibrium in AD patients and healthy controls, as well as difference in time to transient equilibrium between the groups. (b) Mean time to transient equilibrium for all investigated regions in the two groups. * denotes a significant difference between AD and HC (Mann-Whitney test, $p < .05$).
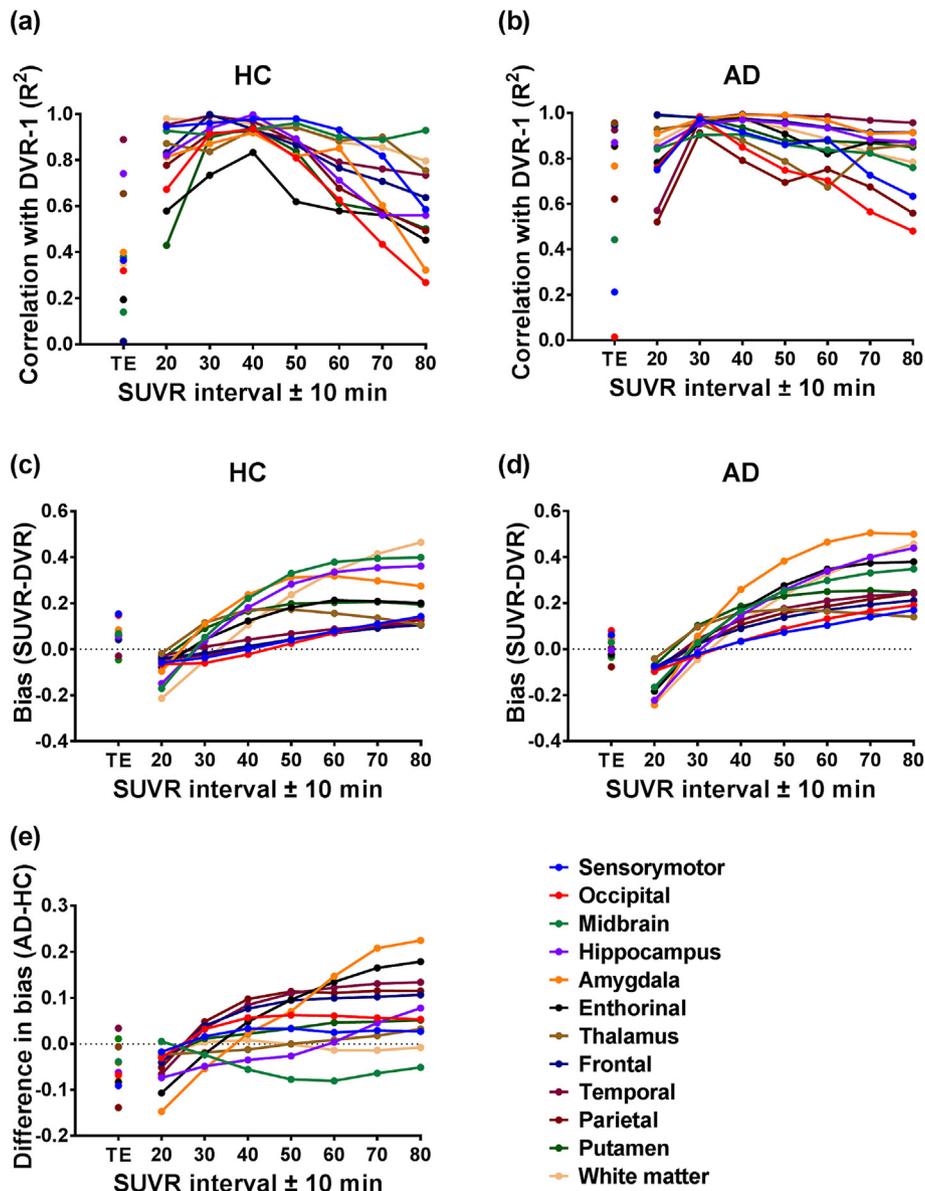

Fig. 3. Correlation between SUVR-1 at various time intervals with DVR-1 in (a) HC and (b) AD; absolute bias of SUVR-1 relative to DVR-1 in (c) HC and (d) AD; and (e) difference in bias relative to DVR-1 between AD and HC.
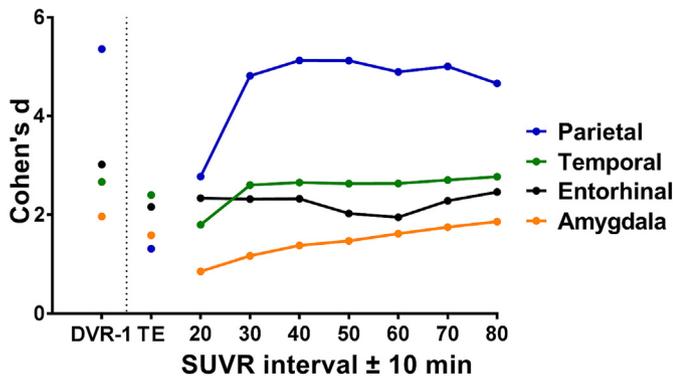
Fig. 4. Cohen's d as a function of DVR-1 and SUVR-1 at TE and different time intervals for parietal-, temporal-, entorhinal cortex and amygdala between AD patients and HCs.
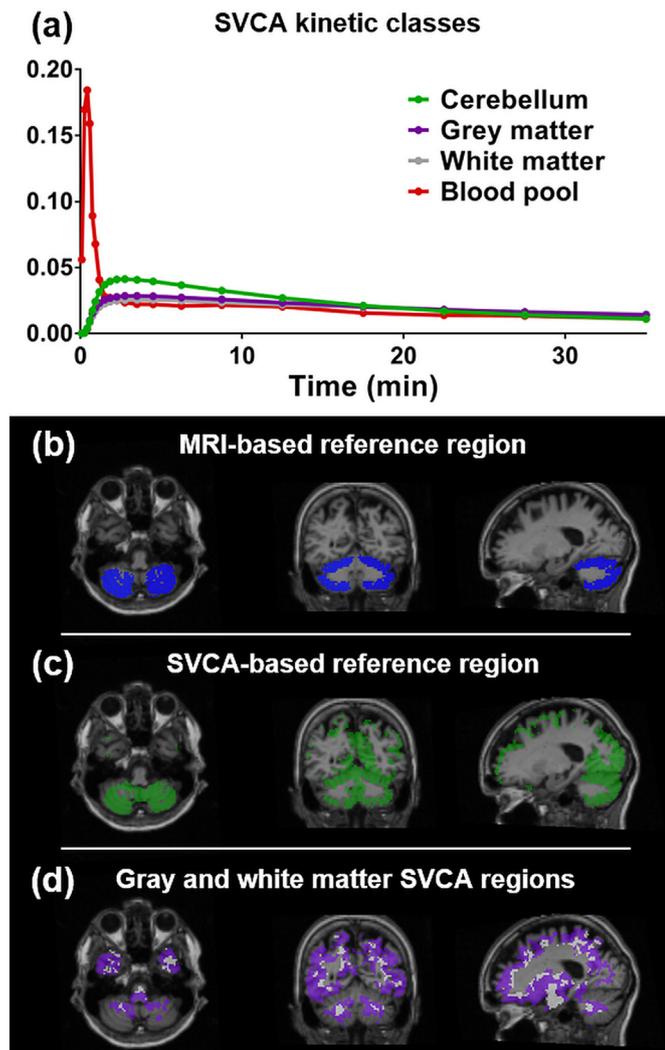

Fig. 5. (a) The predefined kinetic classes used for SVCA as normalized time activity curves, (b) MRI-based cerebellum reference region, (c) reference region extracted using SVCA and (d) grey matter (purple) and white matter (orange) cluster extracted using SVCA where (b-d) are examples from one AD patient. (For interpretation of the references to color in this figure legend, the reader is referred to the web version of this article.)

classes are given in Fig. 5(d). All regions are examples from one AD patient. The MRI-based reference VOI are clearly limited to cerebellum, while the SVCA-reference VOI also included voxels outside the

cerebellum, due to similar kinetics of [18F]THK5317 in these regions as in the cerebellum. No voxels corresponding to the blood class were included, and therefore only grey and white matter VOIs are shown in Fig. 5(d), probably due to high extraction of the tracer and noise in individual blood voxels.

High correlation and agreement was found between SUVR-1 with MRI-based and SVCA-based reference TACs in a 20–40 min interval ($R^2 = 0.93$, slope = 0.95), as shown in Fig. 6(a) and (c). High agreement was also found between R_1 using SRTM, 90 min of data, and MRI-based reference and R_1 using RPM, 40 min of data, and SVCA-based reference ($R^2 = 0.94$ and slope = 1.02), as shown in Fig. 6(b) and (d). Parametric [18F]THK5317 SUVR-1 and R_1 images with MRI-based and SVCA-based reference are shown in Fig. 7 for one AD patient and one HC, and are visually very similar for both SUVR-1 and R_1.

Cohen's d of SUVR-1 20–40 min with SVCA-based reference, between AD patients and HCs, were 1.04 in amygdala, 3.68 in parietal cortex and 2.55 in both temporal- and entorhinal cortex. This is in high agreement with the Cohen's d values for the MRI-based SUVR-1 20–40 min (± 10%), except in parietal cortex where Cohen's d was 4.82 when using the MRI-based reference region.

4. Discussion

In this study, optimal timing for [18F]THK5317 SUVR-1 values, as well as a supervised clustering method to extract a reference region for generation of parametric SUVR-1 and R_1 images were evaluated. Previous work has shown that SUVR-1 using a late time window greatly overestimates tau binding. To address this issue, time to TE and time-dependent bias were calculated in several brain regions. SUVR-1 was also calculated based on fixed time windows on several consecutive 20 min intervals.

The highly varying time to TE across the brain and between AD and HC groups complicates the definition of a generally applicable static scan interval. However, overall, [18F]THK5317 SUVR-1 values correlated and agreed best with DVR-1 values for the 20–40 min interval, both in AD and HCs. Although use of SUVR values at time of TE for each individual VOI leads to equal agreement with DVR-1 in AD patients as for the 20–40 min interval, correlation with DVR-1 was worse than for $SUVR_{20–40}$-1 and SUVR-1 at an early fixed interval is preferred in terms of both feasibility and robustness. $SUVR_{20–40}$-1 allows for optimal semi-quantitative assessment of tau pathology using a single, clinically feasible, 20 min scan. Lockhart and co-workers (Lockhart et al., 2016) found that SUVR over the time interval 40–60 min gave the most stable results, when compared to DVR, for [18F]THK5351. However, they did not assess the magnitude of bias when other intervals were chosen, and only looked at differences between AD and HC within this 40–60 min window. Similar investigations on regional time to TE as presented in this work have been performed for [18F]AV-1451, also showing a high variation across regions (Heurling et al., 2017). In some regions, there were also large variations in TE between subjects, for example in occipital- and sensorimotor cortex in AD patients and frontal- and entorhinal cortex in HCs. This lead to a substantial lower correlation between DVR-1 and SUVR-1 at TE than at any of the fixed time intervals.

As Fig. 3(e) shows, SUVR-1 demonstrates a higher bias in AD patients than in controls in all regions except the midbrain and hippocampus for time intervals later than 40 min, and this difference increases with time. Although variability in SUVR-1 in terms of reduced correlation with DVR-1 also increases with time, the larger relative bias does lead to a better effect size for SUVR-1 values at later time points than for early time points and for DVR-1 in certain regions. For example, Cohen's d in the amygdala increases from 1.3 to 1.9 for SUVR-1 windows of 20–40 and 70–90 min, respectively, compared to 2.0 for DVR-1.

It has recently been shown that administration of a selective MAO-B inhibitor decreased the brain signal of [18F]THK5351, resulting in an overall decrease of SUVR in some cases, although similar reduction of
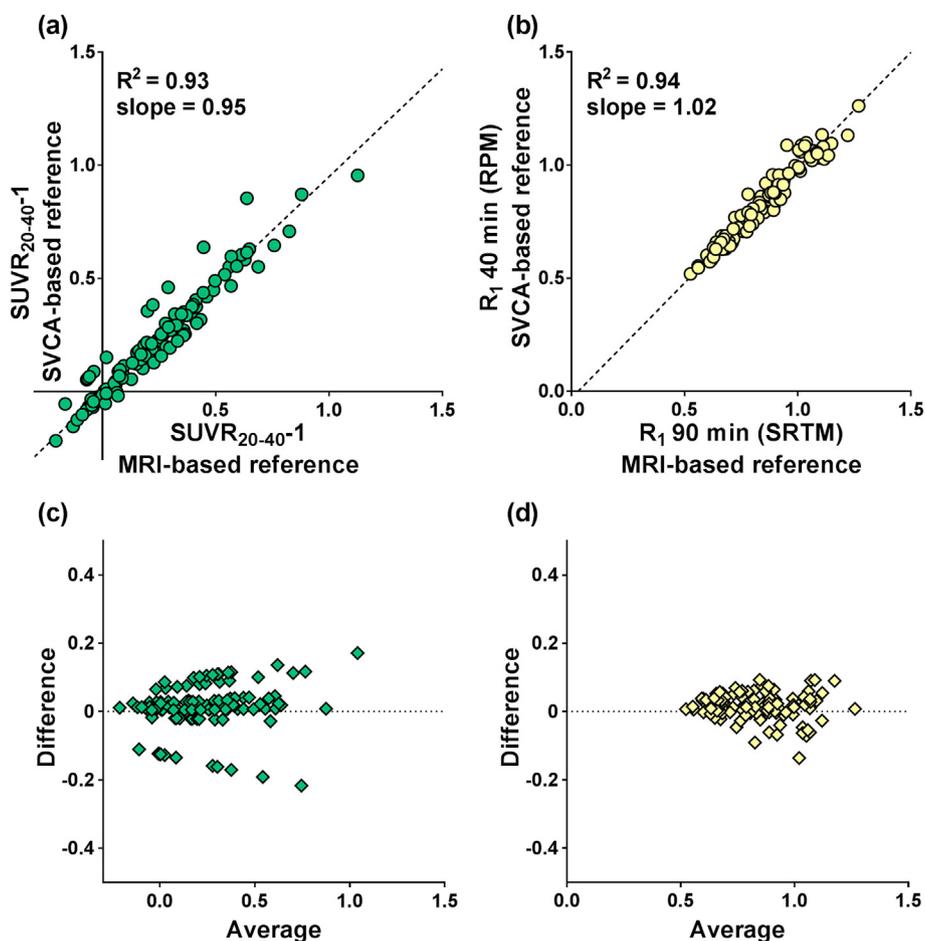
Fig. 6. Relationship between (a) SUVR-1 using the 20–40 min interval with MRI-based cerebellum reference and SVCA-based reference, (b) between 90 min SRTM R_1 with MRI-based cerebellum reference and 40 min RPM R_1 with SVCA-based reference and (c-d) the corresponding Bland-Altman plots.
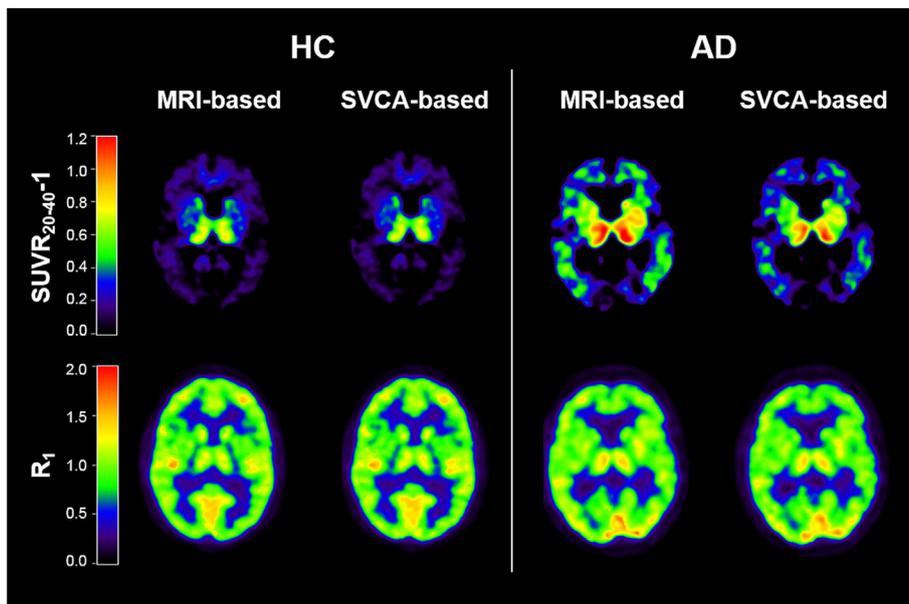

Fig. 7. Example of one HC and one AD patient. On the top row: SUVR-1 of the 20–40 min interval with MRI-based cerebellum reference and the SVCA-based reference and on the bottom row: 90 min R_1 with MRI-based cerebellum reference and 40 min R_1 with SVCA-based reference.

[18F]THK5351 binding in cerebellum may mask this effect.(Ng et al., 2017) Although this effect has not been demonstrated for [18F]THK5317, it would not be unlikely that similar effects may be found for this tracer too, based on the structural similarity and high striatal uptake of both tracers. However, as mentioned in the introduction, *in vitro* studies could not show this effect at concentrations relevant to *in-vivo* studies with [18F]THK5317. Although the results of the present work are not directly applicable to other tau tracers because of differing kinetics, similar issues are likely to be encountered for all other published tau tracers, as mentioned in the introduction, and the optimal window for static imaging should be assessed carefully for each tracer.

SUVR-1 measurements with an SVCA-based reference showed a high agreement to SUVR-1 values with MRI-based reference. SVCA can thus serve as a method to provide a reference TAC directly from the dynamic [18F]THK5317 scan. Even though an MRI in many cases is performed anyway in AD patients, an automatic way of extracting a reference region can still simplify the analysis of dynamic PET data. In addition, since the SVCA method yields a reference region with homogenous kinetics, it may be important in other types of brain injuries with associated tau pathology, such as in patients suffering from brain trauma where the cerebellum may be impaired and cannot be used as reference tissue, and in neurodegenerative diseases where cerebellum is also affected by tau accumulation, such as corticobasal degeneration. In Fig. 6(a) there is a clear line of outliers, all corresponding to the same subject, showing a positive bias in SUVR-1 values when using an SVCA-based reference. This overestimation in SUVR-1 values is due to a poor match of the SVCA reference TAC to the MRI-based cerebellar TAC. In this particular subject, the overestimation would have been reduced if a lower threshold value for inclusion in the reference TAC had been used. A way to further optimize the SVCA algorithm would be to have an individually adaptive threshold, which will be explored in further studies. A possible bias in the implementation of the SVCA is using a total grey matter VOI as one of the cluster classes since it consists of voxels with different amount of specific binding, including regions with no tau accumulation. This will impact the shape of the curve to more resemble the cerebellum curve. However, as seen in Fig. 5(a) there is still a large deviation between the normalized grey matter and cerebellum TACs and since the cluster classes other than cerebellum are only used to avoid inclusion of non-reference voxels in the cerebellum class, this issue is of minor importance. The predefined kinetic classes are based on a rather small group of subjects (4 HC and 4 AD). However, the variation between the normalized tissue curves is small, especially in the cerebellum.

As Rodriguez-Vieitez and co-workers showed, dynamic [18F]THK5317 can measure both tau accumulation as well as R_1, an estimate of the relative cerebral blood flow, with high correlation to [18F]FDG uptake (Rodriguez-Vieitez et al., 2017). As demonstrated in the present work, a scan duration of 40 min is sufficient to measure R_1 using RPM and an SVCA-based reference. Although glucose metabolism and blood flow are obviously not identical measures, dual assessment of binding and relative cerebral blood flow could have clinical value. The possibility of dual-biomarker measurement with [18F]THK5317 could potentially serve as a substitute for [18F]FDG investigations, reducing the number of scans for the patients, and a shorter 40 min scan duration could further facilitate clinical use. In theory, BP_{ND} of the shorter scan duration could also have been investigated using RPM. However, 40 min was not enough to obtain robust BP_{ND} estimates on a voxel level, so this approach was not further investigated.

A possible challenge when using SVCA is that the characteristics of the PET scanner and the reconstruction method may affect the relative shapes of the TACs, making data acquisition and pre-processing routines important. This may complicate the use of such a method in multi-centre studies. A limitation in this study is the low number of subjects included and further studies are needed with patients with pathologies other than AD, where time-dependent bias may vary and the optimal static scan time window may be different.

5. Conclusion

[18F]THK5317 SUVR-1 correlates best to DVR-1 and shows the lowest bias for a time interval of 20–40 min. Use of later scanning times will induce spatially-varying biases in binding estimates and result in overestimation of tau expression in AD patients relative to HCs. High agreement was found between SUVR-1 values, as well as R_1 values, generated with MRI-based cerebellum reference and SVCA-based reference using a 40 min dynamic scan. This suggests that the SVCA method can be used to automatically extract a reference region TAC directly from dynamic [18F]THK5317 PET studies.

Declaration of conflicting interest

The authors declare that they have no conflict of interest.

References

Brix, G., Zaers, J., Adam, L.E., Bellemann, M.E., Ostertag, H., Trojan, H., et al., 1997. Performance evaluation of a whole-body PET scanner using the NEMA protocol. J. Nucl. Med. 38 (10), 1614–1623.

Chiotis, K., Saint-Aubert, L., Savitcheva, I., Jelic, V., Andersen, P., Jonasson, M., et al., 2016. Imaging in-vivo tau pathology in Alzheimer's disease with THK5317 PET in a multimodal paradigm. Eur. J. Nucl. Med. Mol. Imaging 43 (9), 1686–1699.

Chiotis, K., Saint-Aubert, L., Rodriguez-Vieitez, E., Leuzy, A., Almkvist, O., Savitcheva, I., et al., 2018. Longitudinal changes of tau PET imaging in relation to hypometabolism in prodromal and Alzheimer's disease dementia. Mol. Psychiatry 23 (7), 1666–1673.

Golla, S.S., Timmers, T., Ossenkoppele, R., Groot, C., Verfaillie, S., Scheltens, P., et al., 2017. Quantification of Tau load using [18F]AV1451 PET. Mol. Imaging Biol. 19 (6), 963–971.

Gunn, R.N., Lammertsma, A.A., Hume, S.P., Cunningham, V.J., 1997. Parametric imaging of ligand-receptor binding in PET using a simplified reference region model. NeuroImage 6 (4), 279–287.

Hahn, A., Schain, M., Erlandsson, M., Sjolin, P., James, G.M., Strandberg, O.T., et al., 2017. Modeling strategies for quantification of in Vivo 18F-AV-1451 binding in patients with Tau PATHOLOGY. J. Nucl. Med. 58 (4), 623–631.

Heurling, K., Smith, R., Hahn, A., Strandberg, O., Jögi, J., Ohlsson, T., et al., 2017. Regional differences in the transient equilibrium of [18F]AV-1451 and their impact on tissue uptake ratios. In: Alzheimer's Association Internations Conference; July 14–20, 2017; London, England, (P1486–P7).

Ikoma, Y., Edison, P., Ramlackhansingh, A., Brooks, D.J., Turkheimer, F.E., 2013. Reference region automatic extraction in dynamic [(11)C]PIB. J. Cereb. Blood Flow Metab. 33 (11), 1725–1731.

Ito, H., Hietala, J., Blomqvist, G., Halldin, C., Farde, L., 1998. Comparison of the transient equilibrium and continuous infusion method for quantitative PET analysis of [11C] raclopride binding. J. Cereb. Blood Flow Metab. 18 (9), 941–950.

Jonasson, M., Wall, A., Chiotis, K., Saint-Aubert, L., Wilking, H., Sprycha, M., et al., 2016. Tracer Kinetic Analysis of (S)-(1)(8)F-THK5117 as a PET Tracer for Assessing Tau Pathology. J. Nucl. Med. 57 (4), 574–581.

Jonasson, M., Appel, L., Danfors, T., Nyholm, D., Askmark, H., Frick, A., et al., 2017.

Development of a clinically feasible [11C]PE2I PET method for differential diagnosis of parkinsonism using reduced scan duration and automated reference region extraction. Am. J. Nucl. Med. Mol. Imaging 7 (6), 263–274.

Lammertsma, A.A., Hume, S.P., 1996. Simplified reference tissue model for PET receptor studies. NeuroImage 4 (3 Pt 1), 153–158.

Lemoine, L., Saint-Aubert, L., Marutle, A., Antoni, G., Eriksson, J.P., Ghetti, B., et al., 2015. Visualization of regional tau deposits using (3)H-THK5117 in Alzheimer brain tissue. Acta Neuropathol. Commun. 3, 40.

Lemoine, L., Saint-Aubert, L., Nennesmo, I., Gillberg, P.G., Nordberg, A., 2017. Cortical laminar tau deposits and activated astrocytes in Alzheimer's disease visualised by (3) H-THK5117 and (3)H-deprenyl autoradiography. Sci. Rep. 7, 45496.

Lockhart, S.N., Baker, S.L., Okamura, N., Furukawa, K., Ishiki, A., Furumoto, S., et al., 2016. Dynamic PET measures of tau accumulation in cognitively normal older adults and Alzheimer's disease patients measured using [18F] THK-5351. PLoS One 11 (6), e0158460.

Logan, J., Fowler, J.S., Volkow, N.D., Wang, G.J., Ding, Y.S., Alexoff, D.L., 1996. Distribution volume ratios without blood sampling from graphical analysis of PET data. J. Cereb. Blood Flow Metab. 16 (5), 834–840.

Lohith, T., Bennacef, I., Sur, C., Declercq, R., Serdons, K., Bormans, G., et al., 2017. Quantification of [18F]MK-6240, a new PET tracer targeting human neurofibrillary tangles (NFTs) in brain of healthy elderly and subjects with Alzheimer's disease. J. Nucl. Med. 58 (supplement 1), 277.

Lyoo, C.H., Zanotti-Fregonara, P., Zoghbi, S.S., Liow, J.S., Xu, R., Pike, V.W., et al., 2014. Image-derived input function derived from a supervised clustering algorithm: methodology and validation in a clinical protocol using [11C](R)-rolipram. PLoS One 9 (2), e89101.

Ng, K.P., Pascoal, T.A., Mathotaarachchi, S., Therriault, J., Kang, M.S., Shin, M., et al., 2017. Monoamine oxidase B inhibitor, selegiline, reduces (18)F-THK5351 uptake in the human brain. Alzheimers Res. Ther. 9 (1), 25.

Okamura, N., Furumoto, S., Harada, R., Tago, T., Yoshikawa, T., Fodero-Tavoletti, M., et al., 2013. Novel 18F-labeled arylquinoline derivatives for noninvasive imaging of tau pathology in Alzheimer disease. J. Nucl. Med. 54 (8), 1420–1427.

Okamura, N., Harada, R., Furumoto, S., Arai, H., Yanai, K., Tau, Kudo Y., 2014. PET imaging in Alzheimer's disease. Curr. Neurol. Neurosci. Rep. 14 (11), 500.

Rissanen, E., Tuisku, J., Luoto, P., Arponen, E., Johansson, J., Oikonen, V., et al., 2015. Automated reference region extraction and population-based input function for brain [(11)C]TMSX PET image analyses. J. Cereb. Blood Flow Metab. 35 (1), 157–165.

Rodriguez-Vieitez, E., Leuzy, A., Chiotis, K., Saint-Aubert, L., Wall, A., Nordberg, A., 2017. Comparability of [18F]THK5317 and [11C]PIB blood flow proxy images with [18F]FDG positron emission tomography in Alzheimer's disease. J. Cereb. Blood Flow Metab. 37 (2), 740–749.

Svarer, C., Madsen, K., Hasselbalch, S.G., Pinborg, L.H., Haugbol, S., Frokjaer, V.G., et al., 2005. MR-based automatic delineation of volumes of interest in human brain PET images using probability maps. NeuroImage 24 (4), 969–979.

Turkheimer, F.E., Edison, P., Pavese, N., Roncaroli, F., Anderson, A.N., Hammers, A., et al., 2007. Reference and target region modeling of [11C]-(R)-PK11195 brain studies. J. Nucl. Med. 48 (1), 158–167.

Villemagne, V.L., Fodero-Tavoletti, M.T., Masters, C.L., Rowe, C.C., 2015. Tau imaging: early progress and future directions. Lancet Neurol. 14 (1), 114–124.

Yaqub, M., van Berckel, B.N., Schuitemaker, A., Hinz, R., Turkheimer, F.E., Tomasi, G., et al., 2012. Optimization of supervised cluster analysis for extracting reference tissue input curves in (R)-[(11)C]PK11195 brain PET studies. J. Cereb. Blood Flow Metab. 32 (8), 1600–1608.